Time dependencies in the dynamic mechanical behavior of 3D microtissue cell cultures

Condensed Running Title: microtissue viscoelasticity

Matthew Walker[1], Michel Godin[2,3,4], James L. Harden[2,5], Andrew E. Pelling[1,2,6,7]*

[1]Department of Biology, Gendron Hall, 30 Marie Curie, University of Ottawa, Ottawa, ON, K1N5N5 Canada
[2]Department of Physics, 150 Louis Pasteur pvt., STEM Complex, University of Ottawa, Ottawa, ON K1N 6N5 Canada
[3]Department of Mechanical Engineering, Colonel By Hall, 161 Louis Pasteur, University of Ottawa, Ottawa, ON K1N6N5 Canada
[4]Ottawa-Carleton Institute for Biomedical Engineering, Colonel By Hall, 161 Louis Pasteur, University of Ottawa, Ottawa, ON K1N6N5 Canada
[5]Ottawa Institute of Systems Biology, University of Ottawa, Ontario K1H 8M5, Canada
[6]Institute for Science Society and Policy, Simard Hall, 60 University, University of Ottawa, Ottawa, ON, K1N5N5 Canada
[7]SymbioticA, School of Human Sciences, University of Western Australia, Perth, WA, 6009 Australia

Keywords:
Microtissue, Viscoelasticity, Cell mechanics, 3D cell culture, Microfabrication

* Author for correspondence
Andrew E. Pelling
150 Louis Pasteur pvt.
University of Ottawa
Ottawa, ON K1N 6N5
Canada
Tel. +1 613 562 5800 Ext 6965

Fax. +1 613 562 5190

Email: a@pellinglab.net
Web: http://www.pellinglab.net

Abstract

Characterizing the elastic and dissipative properties of cells is not only necessary to determine how they deform, but also to fully understand how external mechanical forces trigger biochemical-signaling cascades to govern their behavior. Presently mechanical properties are largely assessed by applying local shear or compressive forces on single cells in isolation grown on non-physiological 2D surfaces. In comparison, our microfabricated vacuum actuated stretcher measures tensile loading of 3D multicellular 'microtissue' cultures. With our approach, we assessed here the time-dependency of microtissue mechanics and quantified the spatial remodeling that follows step length changes. Unlike previous results from other micro-rheological techniques, stress relaxation and recovery in microtissues followed stretched exponential behaviors that shared similar amplitudes but differed in their dynamics. In that regard, relaxation time constants changed with an inverse power law with step size, while recovery rates were invariant. Pharmacological responses, however, indicated that the contributions of individual cytoskeletal elements did not qualitatively differ from our existing understanding of their roles. The elasticity and dissipation of microtissues were mainly determined by the actin cytoskeleton but also augmented by myosin motor activity and reduced by the presence of microtubules. These results were reflected in changes to remodeling dynamics and spatial distributions of the integrated strain field. This assessment of microtissues offers insights into how the collective behavior of cells and their cytoskeletal proteins generate the dynamic mechanical properties of tissues, which is necessary for a full understanding of how cell behaviors are regulated in both health and disease.

Introduction

The requirements of crawling, dividing and contracting demand that the cell's cytoskeletal network of structural and motor proteins be tremendously dynamic. This behavior is unique from other soft materials and gives cells and tissues their distinct elastic and dissipative properties. Defining these properties is not only necessary for an understanding of how cells deform, but also how cells sense and transduce external mechanical forces into biochemical signals that direct cell behavior. In that regard, when cells are stretched or come in contact with a stiffer matrix, there are time-scale dependent conformational changes to adhesion and cytoskeletal proteins, which in turn alter ligand-receptor binding affinities to trigger biochemical signaling cascades [1,2]. Through this regulation of biochemical signaling, mechanical forces have been linked to normal development and function, as well as disease progression, including bone, muscle, heart and lung disorders and cancer [3,4].

Cells have long been shown to exhibit both solid-like elastic and fluid-like viscous properties depending upon the time-scale at which they are measured [5]. Traditionally this behavior, called viscoelasticity, is described using a network of elastic springs, and viscous dashpots. Solving the constitutive equations for these types of models following a step change in length gives an exponential decay in stress with characteristic time constants depending upon the elastic modulus of the springs and viscosity of the dashpots [6].

Many studies have set out to define the viscoelastic behavior of cells and to link them to specific processes that occur within the cell. Although initial experimental data could be fit with a single time constant [7–10], as the resolution of techniques has improved, fitting the resulting data has required more model parameters [11]. Moreover, exponential-like behavior is not always observed. In particular, a power law with a single exponent was shown to accurately describe both the frequency response and viscoelastic stress relaxation of cells grown on 2D substrates [12–15]. Seemingly universal observations of power law rheology across different cell types, techniques and following a range of cytoskeletal drugs, has since given traction to the hypothesis that cells belong to a class materials called soft glasses [12,13].

Perhaps rather importantly, yet under appreciated, this current understanding of cell mechanics has been mainly shaped by growing cells on 2D substrates with probes applying local shear and compressive loads [12–15]. First in that regard, it is known that forcing un-natural apical-basal polarity of adhesion complexes by growing cells on 2D substrates causes vast differences in the distribution and structure of the cytoskeleton when compared to cells grown within more physiologically relevant 3D environments[16]. It is reasonable to suspect that these fundamental changes to cytoskeletal structure caused by the dimensionality of the cell's environment may alter their mechanical behavior. Secondly, it is reasonable to suspect that an inhomogeneous network of actin, microtubules and cross-linkers will transfer loads differently when probed locally in shear and compression vs. globally in tension. Indeed

when cells have been probed previously in tension at their length-scale, they have exhibited time-scale dependencies that are not captured by power laws typical of other micro-rheological methods[10,17,18].

For these reasons, 3D cell culture methods that enable the assessment of tensile forces have become a keen interest to the field of cell mechanics[19]. In that regard, both the frequency and stress relaxation response of cells within bulk reconstituted collagen gels have previously been fit with a standard linear spring-dashpot models[17,20]. Due to their centimeter-scale, however, these cultures tend to have poor cellular organization and low cell density, suffer from slow experimental throughput, are hard to image, and possess a high diffusive barrier for nutrients. In contrast to bulk 3D cultures, previous microtissue models have been fabricated, consisting of a high throughput array of flexible cantilevers around which cells in a collagen matrix form sub millimeter-scale structures with comparable cell alignment and density to human tissue [21]. Although quasi-static mechanics (i.e. contractility and stiffness) of microtissues have already received attention [21–24], the time-dependencies in these systems remain unclear.

In this article we investigated the viscoelastic stress relaxation of microtissue cultures using a microfabricated device that we have developed called the Microtissue Vacuum Actuated Stretcher (MVAS) [25,26]. The MVAS enables large deformations, and simultaneous measurements of tension and live imaging. The description of the dynamic behavior of 3D microtissue cultures that follows in this article qualitatively differs from local measurements on cells in 2D culture, and thus, raises important questions on how as a field we measure cell mechanics and the models that use to describe them.

Methods

MVAS device

MVAS-force devices were fabricated out of polydimethylsiloxane (PDMS) using mold replication and plasma bonding steps outlined previously[25,26] from three masters created with standard photolithographic techniques. The MVAS-force consists of 60 microtissue wells, each containing two cantilevers spaced apart by 500μm around which the 3D microtissues form (Fig. 1a). A vacuum chamber borders one side of each well and is connected to an external electronic regulator (SMC ITV0010) controlled through Labview software. When a vacuum is applied, the cantilever closest to the vacuum chamber moves to stretch the microtissue, while the other cantilever is used as a passive force sensor by optically tracking its deflection and utilizing its known spring constant ($k_{cantilever}$=0.834N/m). The dimensions of the force sensing cantilever were empirically chosen to be stiff enough to reduce the amount of creep that inherently occurs during stress relaxation because of our method of force measurement, yet also soft enough in order to have a sufficient signal to noise ratio in tension measurements.

Cell culture

NIH3T3 fibroblast (ATCC) cells were cultured in Dulbecco's Modified Eagle's Medium (DMEM) (Hyclone Laboratories Inc.) supplemented with 10% fetal bovine serum (FBS), 50mg/ml streptomycin and 50U/ml penicillin antibiotics (all from Hyclone Laboratories Inc.). Cells were grown at 37℃ with 5% CO_2 on 100mm tissue culture dishes (Fisher) until 80-90% confluent.

Microtissue fabrication

Microtissues consisting of 3T3 fibroblasts in a 3D collagen matrix were cultured as previously described [21,25]. Briefly, the MVAS was sterilized with 70% ethanol, and treated with 0.2% Pluronic F-127 (P6866, Invitrogen) for two minutes to reduce cell adhesion. 250,000 cells were resuspended in 1.5mg/ml rat tail collagen type I (354249, Corning) solution containing 1x DMEM (SH30003.02, Hyclone), 44 mM $NaHCO_3$, 15 mM d-ribose (R9629, Sigma Aldrich), 1% FBS and 1 M NaOH to achieve a final pH of 7.0-7.4. The cell-collagen solution was pipetted into the MVAS and centrifuged to load ~650 cells into each well. The excess collagen was removed and the device was transferred into the incubator for 15 minutes to initiate collagen polymerization. An additional ~130 cells were centrifuged into each well and allowed to adhere to the top of the tissues. Excess cells were washed off. Cell culture media was added and changed every 24 hours.

Imaging

All images were acquired on a TiE A1-R laser scanning confocal microscope (LSCM) (Nikon) with standard LSCM configurations using appropriate laser lines and filter blocks. To assess morphology, microtissues were fixed *in situ* with paraformaldehyde for 10 minutes and permeabilized with 0.5% Triton-X for 3 minutes. The actin cytoskeleton was stained with Alexa Fluor 546 Phalloidin (Fisher, A22283) and the nuclei were stained with DAPI (Fisher, D1306).

Force measurements

After three days of static culture, we measured both stress relaxation of microtissues following a step strain and stress recovery after a subsequent return to initial length at 37°C and 5% CO_2. Changes in microtissue tension were deduced from the visible deflection of the force-sensing cantilever. Bright field images of the tops of the cantilevers were captured at 15 frames per second during both stress relaxation and recovery. The cantilever tops were tracked using pattern matching with adaptive template learning in Labview. To aid in tracking the bottom position of the force-sensing cantilever, the middle device layer was fluorescently labeled by doping the PDMS mixture with Rhodamine-B prior to curing. Fluorescent

images of the bottom of the cantilevers were captured before and after stress relaxation and recovery experiments. After thresholding, the bottom position of the force-sensing cantilever was measured from these images with a simple centroid algorithm in Matlab. The deflection of the force sensor was then calculated by subtracting the difference in the top and bottom positions. A validation of our approach with an elastic standard and characterization of the noise floor are in SI 1.

To investigate nonlinearities in the viscoelastic behavior of microtissues, stress relaxation and recovery were measured for various step strain values. The strain, ε, was defined as the percent change in the length between the innermost edges of the tops of the cantilevers once the microtissue had fully relaxed or recovered (equation 1).

$$\varepsilon(t) = \frac{length(t) - length_o}{length_o} \times 100 \quad (1)$$

To assess the role of individual cytoskeletal proteins in contributing to the viscoelasticity of microtissues, measurements were taken following 20 minute incubations with either 10μM nocodazole (Noco), a microtubule polymerization inhibitor, 5μM blebbistatin (Bleb), a myosin-II inhibitor, 10 μM cytochalasin D (CytoD), an actin polymerization inhibitor, or 0.5% Triton-X, to decellularize microtissues. 0.5% DMSO was used a loading control. As mechanical properties varied between microtissues, each microtissue was compared to its own pre-treatment value where indicated. To prevent crossover in response from multiple drugs, only a single treatment was administrated to any given microtissue.

Quantification of microtissue remodeling

To quantify the spatial distribution of remodeling that occurs following a change in length, local strains were estimated across microtissues using a method described previously [25]. Briefly, starting at the frame immediately following the step change in length, inter-frame displacements were estimated every one second for 100 seconds in Labview at two-pixel spacing across a region of interest using a four level-pyramid based Lucas and Kanade algorithm[27] with sub-pixel precision and a window size of 17x17 pixels. In Matlab, the displacement field was first smoothed with a LOWESS surface-fitting algorithm, then the inter-frame strain tensor was calculated by finding the gradient of the smoothed displacement field, and finally the inter-frame strain tensor was integrated to estimate the local total strain field.

Data analysis and statistics

All numerical data are presented as mean ± standard error. Statistical tests as described in the results were performed using Originlab 8.5 (Northampton, MA), with $p<0.05$ considered statistically significant. Fits to stress relaxation data were performed using Matlab's curve fitting toolbox.

Results

Microtissues are viscoelastic

In the MVAS, cells in a collagen matrix compacted around the cantilevers into freely suspended 3D microtissues with high cell density and organization (fig. 1). In contrast to bulk 3D cell cultures[17,28], the cells in microtissues are mostly aligned with the direction of tension development shown by both the longitudinally oriented actin cytoskeleton and the nuclei in fig. 1b. After three days of static culture, fibroblast microtissues developed a resting tension of 8.7±0.4μN (N=79).

In addition to static tensile measurements, the MVAS enables the assessment of dynamic mechanical behavior through a vacuum-driven planar stretch and by visibly tracking the deflection of the force-sensing cantilever (fig. 1a). Following a step change in length, microtissue tension rose sharply and then relaxed through well-conserved dynamics to a new equilibrium point as commonly seen in viscoelastic solids (fig. 1c). Upon returning the microtissue to its initial length, the tension dropped past and then slowly recovered to its original resting value ($P>0.05$, repeated measures t-tests). This behavior was highly repeatable as subsequent steps were superimposable (SI 2). These results indicate that cells within microtissues work to maintain unique tension equilibriums at any given strain.

In order to further characterize the viscoelastic behavior of microtissues, we searched for an appropriate model to describe their tension (T) relaxation and recovery behavior (fig. 2a and 2b, respectively). First, we tested the standard linear solid (SLS) viscoelasticity model (equation 2) as it has been commonly applied to isolated cells[8–10], 3D cell cultures[17] and ex vivo tissue strips[29]. A SLS model, where k_1 and k_2 are spring constants and τ is a time constant, fits the data well at short time-scales but fails to capture the long time tail in both relaxation and recovery responses.

$$T_{SLS}(t) = \varepsilon\left(k_1 e^{-t/\tau} + k_2\right) \quad (2)$$

In contrast to an exponential model, slow relaxation and recovery at long timescales is exemplified in power law rheological models (equation 3), which been widely reported in single cells[13–15] and tissues [30,31]. For microtissues, a power law, where β is dimensionless constant describing the viscoelastic behavior, fits the slow relaxation at long-timescales but predicts faster than experimental dynamics at shorter times.

$$T_{PL} = \varepsilon\left(k_1 t^{\beta} + k_2\right) \quad (3)$$

From these models it was clear that in order to capture both the exponential stress decay at short-time scales and the slow relaxation at long time-scales, we needed a model that first appeared as an exponential but crossed over to a more slowly relaxing tail behavior at long times. This behavior is characteristic of a stretched exponential (equation 4). Although we have not come across previous reports that have modeled the viscoelastic behavior of cells or tissues with stretched exponentials, they have been widely used to describe relaxation in glassy, disordered systems[32,33]. For microtissues, a stretched

exponential fits both stress relaxation and recovery data over three decades of time (R^2>0.99). The average fitting constants are summarized in table 1. Importantly, the creep that inherently accompanied our method of measuring microtissue tension relaxation was insufficient to significantly change either the type model or the fitting constants (SI 3). While we likely could have fit the data just as well by adding additional exponential time constants to a SLS, as in a Wiechert model[34], this method is an ineffective use of variables compared to a single stretched exponential.

$$T(t) = \varepsilon\left(k_1 e^{-(t/\tau)^{\beta}} + k_2\right) \quad (4)$$

The spring elements, k_1, describing the amplitudes of stress relaxation and recovery, agreed well each other. Moreover, the spatial distributions of strain, describing the locations of stress relaxation and recovery, were well correlated (fig. 2d). This indicates that the regions in the tissue that underwent stress relaxation were also responsible for stress recovery.

The second spring constant (k_2) in equation 4 describes the residual elastic stress in the tissue once fully relaxed or recovered. The source of this elasticity is unclear. It may arise from the contribution of the matrix, or perhaps indicates of the existence of a stress threshold up to which cytoskeletal elements can behave elastically but beyond which they yield. In recovery curves k_2 is approximately equal to zero, indicating that microtissues fully recovered to their original prestress upon returning to their initial length. In other words, any remodeling done to relax the increase in tensile stress that accompanies a step strain, is undone once microtissues are returned to their initial lengths.

In fig. 2c microtissue tension, T, during stress relaxation and recovery was normalized to the respective amplitudes of the responses. By normalizing the curves in this manner, it was clear that relaxation occurred much quicker than stress recovery. Therefore the dynamics of these viscoelastic responses are imbalanced.

In this section we have described the viscoelasticity of microtissues and found that this behavior can be captured through a relatively efficient stretched exponential model. In the rest of this article, we aimed to gain further insight into how the mechanics of microtissues are controlled by underlying molecular and structural mechanisms in the cells by first examining how this behavior is affected by strain, and secondly, how microtissue viscoelasticity changes under a range of pharmacological treatments targeting specific cytoskeletal elements.

Microtissue viscoelasticity is nonlinear

To assess whether there are nonlinearities in the viscoelastic behavior of microtissues, stress relaxation and recovery measurements were performed at various step strain amplitudes on the same tissues. Shown in fig. 3a are average response curves for 3.3 ± 0.2 % and 10.9 ± 0.8% step strains. Using the same method of normalization as above, fig. 3b shows that stress relaxation occurred much more

quickly following larger step strains. In contrast, the rate of stress recovery was step strain amplitude invariant (fig. 3c) and it did not depend upon the strain at which the microtissue recovered (SI 4). Therefore the rate of stress relaxation in microtissues was nonlinear with strain for large amplitudes, while stress recovery was linear for the same range of amplitudes.

The changes to fitting constants for stress relaxation and recovery for these strain amplitudes are summarized in tables 2 and 3 respectively. For stress relaxation, a larger step strain decreased both of the spring constants (repeated measures T-tests; for k_1: $P<0.001$, for k_2: $P<0.05$), the time constant ($P<0.001$) and the power law constant ($P<0.001$). In comparison, for stress recovery, applying a larger step strain only significantly reduced the k_1 spring constant ($P<0.001$). Recovery responses shared the same time, and power law constants, and the tissue tension fully recovered under both small and large step strain sizes (all $P>0.05$).

To further highlight these nonlinearities, the viscoelastic responses in 160 microtissues were analyzed with step strains ranging from 1.75 ± 0.06% to 14.3 ± 0.2%. As reported above, the recovery time constant stayed relatively strain-invariant (fig. 3d). On the other hand, the relaxation time constant decreased with what appeared to be a power law dependence on strain amplitude (non-linear regression: $R^2=0.96$ $P<0.001$), although the range of strain only spanned a single decade. The remaining fitting constants are summarized in SI 5 and 6. As with our repeated-measurement findings, k_1 relaxation and recovery values were weakly correlated to strain (linear regression: $R^2=0.78$ $P<0.001$ and $R^2=0.66$ $P<0.05$, respectively), indicating that on fast time-scales, microtissues strained softened. However, in contrast to repeated-measurements, neither k_2 nor the power law relaxation constant were dependent on strain (linear regression: $P>0.05$), possibly because inter-tissue variance may have outweighed these trends. k_2 and power law constants also seemed to be invariant for stress recovery data (linear regression: $P>0.05$).

In addition to the fitting constants, the spatial distribution of microtissue remodeling following a step change in length varied considerably with strain. Fig. 4a and b show, respectively, the raw and normalized remodeling in the transverse direction in representative microtissues after 100 seconds. Remodeling during stress relaxation and recovery in the transverse direction increased with step size and became transversely focused to the center of the tissue but longitudinally diffuse, spanning the entire tissue length.

Transverse strain fields were averaged across the region of interest to compute a mean metric of the integrated remodeling response through time (fig. 4c and d, respectively). During stress relaxation following a small step strain (1.7 ± 0.2%), microtissues showed little remodeling in the transverse direction. With an intermediate step strain (3.4 ± 0.2%), microtissues relaxed to reach a new equilibrium. Lastly, with a large step strain (10.4 ± 0.5%), microtissues quickly relaxed, then contracted to a smaller degree, and eventually reached an equilibrium strain.

Mean recovery curves showed slower dynamics (fig. 4d) compared to relaxation curves. Yet, relaxation and recovery following small and intermediate step strains shared similar spatial distributions and amplitudes but with opposing signs, indicating that the gross structural remodeling that occurred after a step strain is in part reversible. In contrast however, recovery amplitudes following a large step strain were comparably higher than the final equilibrium in relaxation curves. This suggests that large steps sizes may cause permanent remodeling in microtissues through a stretch activated contraction.

In comparison with the remodeling in the transverse direction, remodeling in the longitudinal direction was less extensive being constrained by the cantilevers. Longitudinal remodeling was also highly tissue-specific and mainly located near the fronts of the cantilevers rather than the body of the tissue. This behavior likely was not indicative of tissue detachment from the cantilevers but rather reflected the heterogeneity and anisotropy within microtissue cultures as final relaxation and recovery longitudinal strain fields shared similar mean amplitudes for all tested step sizes (SI 7).

Pharmacological behaviors

To assess the role of several key cellular proteins in governing microtissue viscoelasticity, stress relaxation and recovery were measured following various pharmacological treatments meant to either disrupt the cytoskeleton or alter actomyosin activity. Normalized responses and fitting constants are shown in fig. 5a and table 4, respectively. Each fitting constant was normalized and compared with paired t-tests to their own pre-treatment control. DMSO was used as a loading control and did not affect either relaxation or recovery curves. Furthermore none of the treatments caused a difference between the initial tension prior to a step strain and the final tension following stress recovery, indicating that there was no plastic change to the microtissues and that the incubation periods for the treatments were sufficient to reach an equilibrium state.

Consistent with our understanding that microtubules act as compressive struts that oppose actomyosin activity [35], microtubule depolymerization with nocodazole increased the resting tension in microtissues by 3.7 ± 0.4μN ($P<0.001$). Microtissue spring constants for stress relaxation (k_1 and k_2 both $P<0.001$) and recovery (k_1 $P<0.001$) responses increased as well. Microtubule depolymerization did not effect either the time or power law constants for stress relaxation (τ and β both $P>0.05$). However, in contrast, nocodazole treatment increased the time constant, τ, and decreased the power law constant, β for stress recovery ($P<0.01$ and $P<0.05$, respectively). This suggests that the recovery rate may be altered through the regulatory action of microtubules on acto-myosin activity, but that relaxation rates are unchanged.

Myosin inhibition (blebbistatin), actin depolymerization (cytochalasin D) and decellularization (triton-X) all decreased resting microtissue tension (by -2.8 ± 0.5 μN, -5.0 ± 0.4μN and -8.8 ± 0.8μN, respectively; all $P<0.001$), relaxation k_1 and k_2, and recovery k_1 (various P values). Blebbistatin treatment

did not affect the relaxation time constant but did decrease the recovery time constant ($P<0.01$), indicating again that myosin motor activity, in part, determines the recovery speed. There was no observable stress relaxation or recovery upon either actin depolymerization or decellularization, and for this reason, it was not possible to accurately fit time and power law constants to these treatments. Nevertheless, these curves show that remodeling in actin microfilaments is chiefly reasonable for the viscoelastic behavior of microtissues.

To examine how microtissue remodeling during relaxation and recovery was affected by microtubules, actin microfilaments, myosin motor activity and the extracellular matrix, strain fields were assessed at the same small step strain (1.7 ± 0.2%) following pharmacological treatments. Microtubule depolymerization and myosin inhibition behaved similarly to control microtissues in their transverse (fig. 5b-d) and longitudinal (SI 8) remodeling responses. In contrast, actin depolymerization and decellularization induced remodeling responses that were more consistent with a larger step strain in terms of the spatial distribution, amplitude and dynamics of the strain fields. This finding implicates the depolymerization of actin and the contribution from the matrix in the gross remodeling behavior and nonlinear dynamics observed with large strains.

Discussion

In this article, we assessed the dynamic mechanical behavior of physiologically relevant 3D microtissue cell cultures. As expected, microtissues displayed timescale-varying mechanics. In response to a step increase in length, the tension quickly rose and then relaxed to a new equilibrium point as in a viscoelastic solid. When microtissues were returned to their initial lengths by a recovery strain, their tension quickly dropped below initial measurements, and then slowly, yet fully, recovered. These responses, however, differed greatly in their dynamics. Whereas recovery rates were strain independent, relaxation was a highly nonlinear function of strain, following with what appeared to be an inverse power law with strain amplitude. Both these responses differed from the weak power laws that describe the relaxation of cells in 2D culture typically observed with other micro-rheological techniques [12,13,15]. Therefore, our findings raise important questions about how we characterize the mechanical behavior of cells (globally vs. locally or tension vs. shear vs. compression) and the environment in which they are assessed (2D vs. 3D culture) [36].

In particular, unlike previous work in 2D cell culture, which predominately have used power law models [12,13,15], we found that tensile stress relaxation and recovery in microtissues followed stretched exponential functions. To the best of our knowledge, stretched exponentials have not been previously used to describe the viscoelastic behavior of cells or cell cultures. Still, however, our findings are in close agreement with previous reports from bulk fibroblast populated collagen gels [17,18]. In that regard, we

both reported characteristic time constants of similar magnitudes with time-dependencies that are more broadly distributed than what can be explained by a single exponential function (ie. a SLS model).

In the contrary, there does exist a strong precedent for the use of stretched exponentials to describe relaxation in disordered condensed matter physics. In fact both polymer networks [37] and glasses near their transition temperature [32,33] relax according to stretch exponentials. Such glassy polymer response has already been linked to the mechanical behavior of the cytoskeleton [11]. Furthermore, our average values of β (0.64 ± 0.01 and 0.61 ± 0.01 for relaxation and recovery, respectively) are in close agreement with an universal experimental value of 0.6 in glasses dominated by Brownian motion [38], which is theoretical justified by a so-called 'trapping model' [39]. Mathematically this model is beyond the scope of this work but it is relatively easy to conceptualize. In a trapping model, the material consists of randomly distributed traps. During relaxation, these traps capture molecules that diffuse through the material, and as the traps are filled, the remaining molecules must travel longer to find unoccupied traps. Thereby, the relaxation rate falls with a power law given by the dimensionality of the model.

Although a trapping model can be a great tool to conceptualize stretched exponentials, the question remains whether we can draw out any physiological meaning or link any mechanism(s) to account for the stretched exponential relaxation and recovery in microtissue behavior. Similar to power laws, stretched exponentials can be expanded into a superposition of simple exponential functions with a nontrivial distribution of relaxation times [40]. It should also not be overly surprising that relaxation processes exist across a broad spectrum of timescales in something as complex and heterogeneous as the network of cytoskeletal proteins inside single cells, and in a more collective sense, when considering an aggregate of cells and extracellular matrix. Thus, our fitting constants may be interpreted as a general description of microtissue behavior reflecting the broad viscoelastic heterogeneity in the cytoskeleton and amongst cells rather than capturing a specific process.

In spite of the generality of stretched exponentials, the relaxation spring constants in our model (k_1 and k_2) were tightly coupled throughout an assortment of pharmacological treatments targeting specific proteins, and as well in measurements at different step strain amplitudes; in particular, all treatments followed a single linear relationship (fig. 6a). This coupling behavior has previously been interpreted as evidence suggesting that elastic and dissipative stresses are borne from the same origin(s) [41,42]. Even so, it is surprising that targeting different cytoskeletal elements can produce responses that seemed to follow a single universal relationship, unless an understanding of mechanisms at a hierarchy beyond the single protein-level is required. Rather than following responses in single molecules, as our field has been studying in a traditional reductionist approach, the viscoelasticity of cells and tissues is perhaps more influenced by the association and interaction of proteins with each other [43]. Further evidence in support of this view has been reported through various universalities in single cell mechanics [12,35,44,45].

Dissipative stresses during microtissue relaxation were also strongly coupled to the stress regained during recovery (fig. 6b). Furthermore, for the most part, microtissue remodeling during relaxation and recovery occurred with similar spatial distributions and comparable amplitudes. These results suggest that stress relaxation and recovery depended upon reversible remodeling in the same cells within the microtissue. On the other hand, the dynamics of the relaxation and recovery responses were, for the most part, very different. Relaxation rates were nonlinear with step strain amplitude, decreasing with what appeared to be a power law, but were relatively invariant with microtubule depolymerization or myosin inhibition. In contrast, recovery rates were invariant with step strain amplitude but increased with microtubule depolymerization and decreased with myosin inhibition. This suggests that myosin contributed only as a passive cross-linker during relaxation, while active myosin crossbridge cycling was partially responsible for stress recovery. Still however, the actin cytoskeleton was the principal source of elasticity and dissipation since depolymerization of actin filaments had the biggest effect on microtissue viscoelasticity outside of decellularization. There also appeared to be some passive component to the recovery as there was remodeling upon returning samples with actin-depolymerized cells and as well as in decellularized microtissues to initial lengths. Interestingly, this remodeling was consistent with larger step strains, suggesting that the loss of the actin cytoskeleton and how the cells associate with the matrix may be in part be responsible for the non-linear relaxation rates.

It is not uncommon for relaxation in soft biological tissues to be nonlinear. Perhaps, it is more surprising that stress recovery was so linearly independent of the step strain. Indeed nonlinearities have been previously reported in lung[46], heart valve[47], ligament[48], and muscle[49]. Recently, nonlinear relaxation rates in cells were argued to arise from a poroelastic effect occurring through the redistribution of the viscous cytosolic fluid between local regions within the network of cytoskeletal filaments[50]. It is, however, debatable that the same effect is the main determinant in our measurements, as there is a difference of more than a decade in time-constants between our findings and those of the poroelastic model. Moreover, poroelasticity does not offer an explanation as to why the recovery rates were linear with strain amplitude and much slower than relaxation rates.

An alternative mechanism conceives stress relaxation in cells as a friction force produced by cytoskeletal filaments sliding smoothly past one another [51]. The main support for this hypothesis is that local shear measurements on cells in 2D culture follow the structural damping law; the ratio of dissipative to elastic stresses is invariant of the time-scale at which they are assessed [12,13]. This hypothesis, however, does not offer any explanation as to the nonlinearity observed in relaxation rates and the imbalance with recovery dynamics. Furthermore it is not compatible with either standard linear solid viscoelasticity or a stretched exponential, as both models produce characteristic rate-dependencies that contradict structural damping. Interestingly, in contrast with local shear measurements, characteristic rate-dependencies similar to our observations in microtissues have been previously reported in individual cells[10] and 3D

cultures[17] when probed in tension at a length-scale of the entire cell/culture. It would still be of interest, however, in future work to show that the frequency response of microtissues is consistent with their stretched exponential relaxation in the time domain.

A last possible mechanism to explain the viscoelastic response in microtissues is that stress relaxation and recovery reflects the rupturing and reforming of bonds within the cytoskeleton (i.e. within actin filaments and between actin and its crosslinkers), and between the cells and the extracellular matrix. In support of this hypothesis, there is a strong precedent that mechanical stretch depolymerizes actin filaments[44,52–54] and perturbs myosin binding[55–59]. Indeed, we have shown here that microtissues strain-soften. Further in regard to this hypothesis, the imbalance in microtissue relaxation and recovery rates can simply be explained by differences in bond destruction and formation rates; it is not unreasonable to suspect that it takes less time to pull bonds apart than for proteins in a cell to diffuse through Brownian motion, correctly reorient themselves, and then lastly reform chemical bonds, especially if additional enzymes (ie. profilin) and molecules (ie. ATP) are needed. Furthermore, nonlinearities in relaxation behavior have previously been captured by models in which stress is relieved through sequential rupturing of Maxwell bodies, where each micro-yield event passes the stress on to other regions of the tissue [60,61]. Results from these models give an exponential with a long-tail power law, however it is possible that chemical bonds have a finite yield strength, and therefore in actuality curves may flatten, behaving as stretched exponentials. Admittedly, however, this model is currently unable to explain nonlinearities beyond quasi-linearity, such as the inverse power law between relaxation rate and strain amplitude that we observed.

Conclusions

The viscoelastic behavior of microtissues likely does not come down to a single physiological mechanism, but rather it is an amalgamation of many physical remodeling events occurring at different time and length scales. Therefore, the measured stress relaxation and recovery of microtissues are generalized responses, and perhaps unsurprisingly differ from local measurements in 2D culture. In that regard, we found that the viscoelastic behavior of microtissues followed a stretched exponential, and that stress relaxation rates were nonlinear and imbalanced with a linear recovery response. On the other hand, the contributions of specific cytoskeletal elements (actin, myosin, microtubules) to microtissue mechanics did not qualitatively differ from our previous understanding of their roles in the mechanical behavior of cells grown on 2D substrates. Importantly, all our results, collapsed onto a single relationship between elastic and dissipative stresses, indicating that the cytoskeleton of cells within microtissues may follow an universal behavior set not by the role of individual proteins but rather by the physical architecture of cells and their surrounding matrix as a whole. To conclude, the assessment of dynamic mechanics of microtissues has yielded further insights into how tissues gain their mechanical properties

from cells, and from the distribution and interaction of their cytoskeletal proteins. This knowledge is critical to a full understanding of how physical forces are sensed and regulate cell behavior in health and disease.

Additional Information

Conflicts of Interest

There are no conflicts to declare.

Acknowledgements

M.W. is supported by OGS (Ontario Graduate Scholarship). The authors acknowledge support from individual NSERC Discovery Grants (M.G. and A.E.P.). M.G. and A.E.P. acknowledge the Canadian Foundation for Innovation.

Data Availability

The data generated during the current study is available from the corresponding author upon reasonable request.

References

1 R. D. Kamm and M. R. Kaazempur-Mofrad, *Mech. Chem. Biosyst.*, 2004, **1**, 201–9.

2 D. E. Ingber, *FASEB J.*, 2006, **20**, 811–27.

3 T. Mammoto, A. Mammoto and D. E. Ingber, *Annu. Rev. Cell Dev. Biol.*, 2013, 29, 27–61.

4 D. E. Ingber, *Ann. Med.*, 2003, **35**, 564–77.

5 F. Crick and A. F. W. Hughes, *Exp Cell Res*, 1950.

6 J. McElhaney, *Med. Phys.*, 1982, **9**, 788–789.

7 N. Wang and D. E. Ingber, *Biophys. J.*, 1994, **66**, 2181–2189.

8 G. W. Schmid-Schönbein, K. L. Sung, H. Tözeren, R. Skalak and S. Chien, *Biophys. J.*, 1981, **36**, 243–56.

9 M. Sato, N. Ohshima and R. M. Nerem, *J. Biomech.*, 1996, **29**, 461–467.

10 O. Thoumine and A. Ott, *J. Cell Sci.*, 1997, **110 (Pt 17)**, 2109–16.

11 P. Kollmannsberger and B. Fabry, *Annu. Rev. Mater. Res.*, 2011, **41**, 75–97.

12 B. Fabry, G. N. Maksym, J. P. Butler, M. Glogauer, D. Navajas and J. J. Fredberg, *Phys Rev Lett*, 2001, **87**, 148102.

13 B. Fabry, G. N. Maksym, J. P. Butler, M. Glogauer, D. Navajas, N. A. Taback, E. J. Millet and J. J. Fredberg, *Phys Rev E Stat Nonlin Soft Matter Phys*, 2003, **68**, 41914.

14 J. Alcaraz, L. Buscemi, M. Grabulosa, X. Trepat, B. Fabry, R. Farré and D. Navajas, *Biophys. J.*, 2003, **84**, 2071–2079.

15 B. D. Hoffman, G. Massiera, K. M. Van Citters, J. C. Crocker, K. M. Van Citters and J. C. Crocker, *Proc. Natl Acad. Sci. Usa*, 2006, **103**, 10259–10264.

16 K. M. Hakkinen, J. S. Harunaga, A. D. Doyle and K. M. Yamada, *Tissue Eng. Part A*, 2011, **17**, 713–24.

17 T. Wakatsuki, M. S. Kolodney, G. I. Zahalak and E. L. Elson, *Biophys. J.*, 2000, **79**, 2353–68.

18 J. E. Wagenseil, T. Wakatsuki, R. J. Okamoto, G. I. Zahalak and E. L. Elson, *J. Biomech. Eng.*, 2003, **125**, 719.

19 K. L. Billiar, Springer, Berlin, Heidelberg, 2010, pp. 201–245.

20 R. T. Tranquillo, M. A. Durrani and A. G. Moon, *Cytotechnology*, 1992, **10**, 225–50.

21 W. R. Legant, A. Pathak, M. T. Yang, V. S. Deshpande, R. M. McMeeking and C. S. Chen, *Proc. Natl. Acad. Sci. U. S. A.*, 2009, **106**, 10097–10102.

22 A. R. West, N. Zaman, D. J. Cole, M. J. Walker, W. R. Legant, T. Boudou, C. S. Chen, J. T. Favreau, G. R. Gaudette, E. A. Cowley and G. N. Maksym, *Am J Physiol Lung Cell Mol Physiol*, 2013, **304**, L4–16.

23 R. Zhao, T. Boudou, W.-G. Wang, C. S. Chen, D. H. Reich, Dr., C. S. Chen, Prof., D. H. Reich, Prof., R. B. Zhao Thomas; Wang, Wei-Gang; Chen, Christopher S; Reich, Daniel H;, R. Zhao, T. Boudou, W.-G. Wang, C. S. Chen and D. H. Reich, *Adv. Mater.*, 2013, **25**, 1699–1705.

24 F. Xu, R. Zhao, A. S. Liu, T. Metz, Y. Shi, P. Bose and D. H. Reich, *Lab Chip*, 2015, **15**, 2496–503.

25 M. Walker, M. Godin and A. E. Pelling, *Biomed. Microdevices*, 2018, **20**, 43.

26 M. Walker, P. Rizzuto, M. Godin and A. E. Pelling, *bioRxiv*, 2019, 780312.

27 B. D. . K. Lucas T., B. D. Lucas and T. Kanade, in *Proceedings of the International Joint Conference on Artificial Intelligence*, Morgan Kaufmann Publishers Inc., Vancouver, British Columbia, 1981, pp. 674–679.

28 J. Eyckmans and C. S. Chen, *Comment. Spec. ISSUE 3D CELL Biol.*, 2017.

29 Y. C. Fung, *Biomechanics: Mechanical Properties of Living Tissues*, Springer-Verlag, New York, 1981.

30 J. Hildebrandt, *Bull. Math. Biophys.*, 1969, **31**, 651–67.

31 Y. Fung, *Elasticity of soft tissues in simple elongation*, 1967, vol. 213.

32 R. Rambousky, M. Moske and K. Samwer, *Zeitschrift für Phys. B Condens. Matter*, 1995, **99**, 387–391.

33 K. Schröter and E. Donth, *J. Non. Cryst. Solids*, 2002, **307-310**, 270–280.

34 E. Wiechert, *Ann. Phys.*, 1893, **286**, 546–570.

35 N. Wang, K. Naruse, D. Stamenović, J. J. Fredberg, S. M. Mijailovich, I. M. Tolić-Nørrelykke, T. Polte, R. Mannix and D. E. Ingber, *Proc. Natl. Acad. Sci. U. S. A.*, 2001, **98**, 7765–70.

36 J. Guck, *Biophys. Rev.*, 2019, 11, 667–670.

37 F. Meng, R. H. Pritchard and E. M. Terentjev, *Macromolecules*, 2016, **49**, 2843–2852.

38 G. G. Naumis and J. C. Phillips, *J. Non. Cryst. Solids*, 2012, **358**, 893–897.

39 J. C. Phillips, *Reports Prog. Phys.*, 1996, **59**, 1133–1207.

40 C. P. Lindsey and G. D. Patterson, *J. Chem. Phys.*, 1980, **73**, 3348–3357.

41 J. J. Fredberg and A. Dimitrije, *J Appl Physiol*, 1989, **67**, 2408–19.

42 J. J. Fredberg, D. Bunk, E. Ingenito and S. A. Shore, *J. Appl. Physiol.*, 1993, **74**, 1387–1397.

43 J. Fredberg and B. Fabry, in *Cytoskeletal Mechanics*, eds. M. R. K. Mofrad and R. D. Kamm, Cambridge University Press, Cambridge, 2006, pp. 50–70.

44 X. Trepat, L. Deng, S. S. An, D. Navajas, D. J. Tschumperlin, W. T. Gerthoffer, J. P. Butler and J. J. Fredberg, *Nature*, 2007, **447**, 592–595.

45 X. Trepat, G. Lenormand and J. J. Fredberg, *Soft Matter*, 2008, **4**, 1750.

46 J. H. Bates, G. N. Maksym, D. Navajas and B. Suki, *Ann. Biomed. Eng.*, 1994, **22**, 674–81.

47 T. C. Doehring, E. O. Carew and I. Vesely, *Ann. Biomed. Eng.*, 2004, **32**, 223–32.

48 P. Provenzano, R. Lakes, T. Keenan and R. Vanderby, Jr., *Ann. Biomed. Eng.*, 2001, **29**, 908–914.

49 D. Navajas, S. Mijailovich, G. M. Glass, D. Stamenovic and J. J. Fredberg, *J. Appl. Physiol.*, 1992, **73**, 2681–2692.

50 E. Moeendarbary, L. Valon, M. Fritzsche, A. R. Harris, D. A. Moulding, A. J. Thrasher, E. Stride, L. Mahadevan and G. T. Charras, *Nat. Mater.*, 2013, **12**, 253–261.

51 J. J. Fredberg, K. A. Jones, M. Nathan, S. Raboudi, Y. S. Prakash, S. A. Shore, J. P. Butler and G. C.

Sieck, *J. Appl. Physiol.*, 1996, **81**, 2703–2703.

52 N. Pender and C. A. A. McCulloch, *J. Cell Sci.*, 1991, **100**, 187–93.

53 K. D. Costa, W. J. Hucker and F. C.-P. Yin, *Cell Motil. Cytoskeleton*, 2002, **52**, 266–274.

54 C. Chen, R. Krishnan, E. Zhou, A. Ramachandran, D. Tambe, K. Rajendran, R. M. Adam, L. Deng and J. J. Fredberg, 2010, **5**, e12035.

55 C. Semmrich, T. Storz, J. Glaser, R. Merkel, A. R. Bausch and K. Kroy, *Proc. Natl. Acad. Sci. U. S. A.*, 2007, **104**, 20199–203.

56 D. Humphrey, C. Duggan, D. Saha, D. Smith and J. Käs, *Nature*, 2002, **416**, 413–416.

57 D. Smith, F. Ziebert, D. Humphrey, C. Duggan, M. Steinbeck, W. Zimmermann and J. Käs, *Biophys. J.*, 2007, **93**, 4445–4452.

58 J. J. Fredberg, D. S. Inouye, S. M. Mijailovich and J. P. Butler, *Am J Respir Crit Care Med*, 1999, **159**, 959–967.

59 J. J. Fredberg, D. Inouye, B. Miller, M. Nathan, S. Jafari, S. H. Raboudi, J. P. Butler and S. A. Shore, *Am J Respir Crit Care Med*, 1997, **156**, 1752–1759.

60 J. H. T. Bates, *Ann. Biomed. Eng.*, 2007, **35**, 1165–1174.

61 J. H. T. Bates and B. Ma, *Ann. Biomed. Eng.*, 2013, **41**, 1129–1138.

Table 1: The stress relaxation and recovery fitting constants (N=79).

	k_1 (μN/%)	k_2 (μN/%)	τ (s)	β
Relaxation	0.55 ± 0.03	0.42 ± 0.02	14 ± 1	0.70 ± 0.03
Recovery	0.5 ± 0.02	-0.02 ± 0.02	31 ± 2	0.59 ± 0.02

Table 2: The changes to stress relaxation fitting constants measured at 10.9% vs. 3.3% strain. Values were compared with repeated measures t-tests (N=17) (* P<0.05, ***P<0.001).

Δk_1 (%)	Δk_2 (%)	Δτ (%)	β (%)
-24 ± 4 (***)	-12 ± 5 (*)	-58 ± 5 (***)	-19 ± 5 (***)

Table 3: The changes to stress recovery fitting constants measured at 10.9% vs. 3.3% strain. Values were compared with repeated measures t-tests (N=17) (** P<0.01).

Δk_1 (%)	Δτ (%)	β (%)	$\Delta T_{f\text{-}i}$ (μN)
-28 ± 5 (**)	15 ± 7	-2 ± 3	-0.4 ± 0.2

Table 4: The pharmacologically induced changes to stress relaxation and recovery fitting constants. Each treatment was compared to its pretreatment control using paired t-tests (* P<0.05, ** P<0.01, ***P<0.001).

	ΔT_{base} (μN)	Relaxation				Recovery			
		Δk_1 (%)	Δk_2 (%)	Δτ (%)	Δβ (%)	Δk_1 (%)	Δτ (%)	Δβ (%)	$\Delta T_{f\text{-}i}$ (μN)
Noco (N=24)	3.7 ± 0.4 (***)	40 ± 9 (***)	37 ± 9 (***)	10 ± 12	11 ± 5	96 ± 14 (***)	87 ± 25 (**)	-7 ± 4 (*)	0.03± 0.07
DMSO (N=21)	-0.1 ± 0.2	6 ± 6	8 ± 7	4 ± 9	8 ± 8	10 ± 9	5 ± 13	8 ± 5	0.17 ± 0.09
Bleb (N=16)	-2.8± 0.5 (***)	-27 ± 7 (**)	-15 ± 5 (*)	14 ± 10	-2 ± 9	-32 ± 5 (***)	-27 ± 8 (**)	7 ± 4	-0.1 ± 0.06
CytoD (N=8)	-5.0 ± 0.4 (***)	-74 ± 10 (***)	-47 ± 12 (***)	-	-	-112 ± 6 (***)	-	-	-0.1 ± 0.1
TX (N=7)	-8.8 ± 0.8 (***)	-86 ± 6 (***)	-65 ± 7 (**)	-	-	-109 ± 10 (***)	-	-	-0.1 ± 0.2

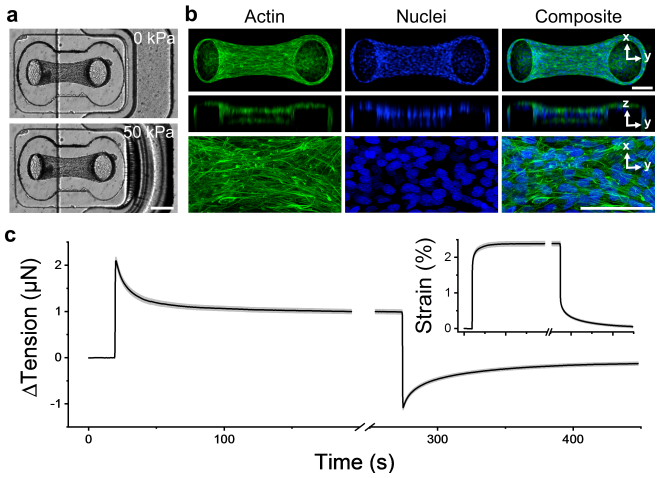

Fig. 1: Microtissue tension dynamically relaxed and recovered with changes in length. Microtissues were grown in our MVAS-force device (a). In the MVAS-force, changes to microtissue length are driven by applying a regulated vacuum pressure to a chamber that borders one side of each microtissue well. The cantilever closest to the vacuum chamber (shown here on the right) is actuated to stretch the microtissue in plane while changes in tension can then be measured by tracking the deflection of the opposing cantilever (on the left). Microtissues are organized 3D cell cultures freely suspended between the cantilevers. Max projections of confocal stacks, orthogonal views and high magnification images are shown in (b). Both the actin cytoskeleton (green), and the nuclei (blue) are predominately aligned between the cantilevers. Scale bars in (a) and (b) represent 200μm and 100μm, respectively. Following a step in strain (insert), microtissue tension (N=79) sharply increased and then relaxed to a new set point as expected in a viscoelastic solid (c). Then upon returning the microtissue to its original length, the tension recovered.

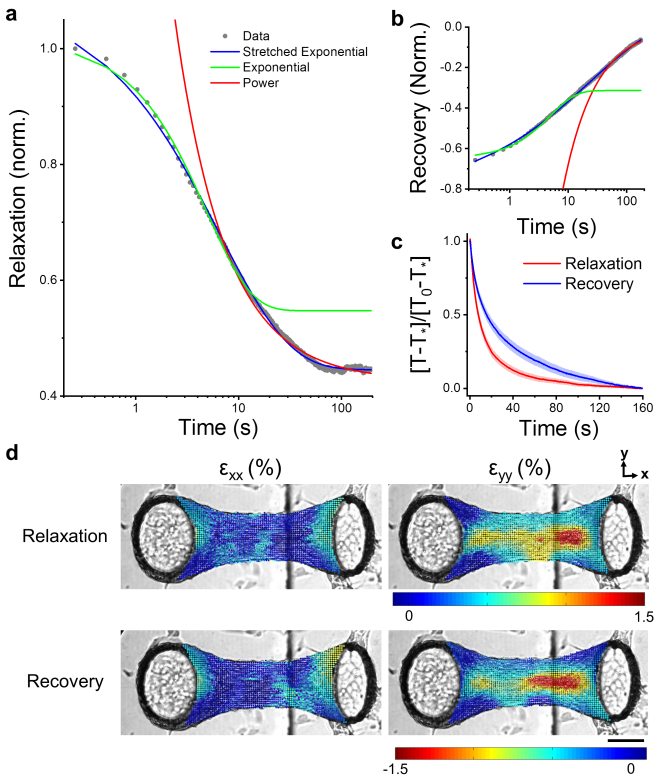

Fig. 2: Stress relaxation and recovery in microtissues followed stretched exponential trajectories. Microtissue stress relaxation fitted to various viscoelastic models is shown in (a) and stress recovery is shown in (b). Stretched exponentials capture relaxation and recovery behaviors over three decades of time. Responses are normalized to their amplitudes in (c), showing that relaxation occurred much quicker than stress recovery. Yet, stress relaxation and recovery appeared to share the same spatial locations within a given microtissue in terms of both remodeling in the longitudinal (ε_{xx}) and transverse (ε_{yy}) directions immediately following the change in length (d). The scale bar represents 100μm.

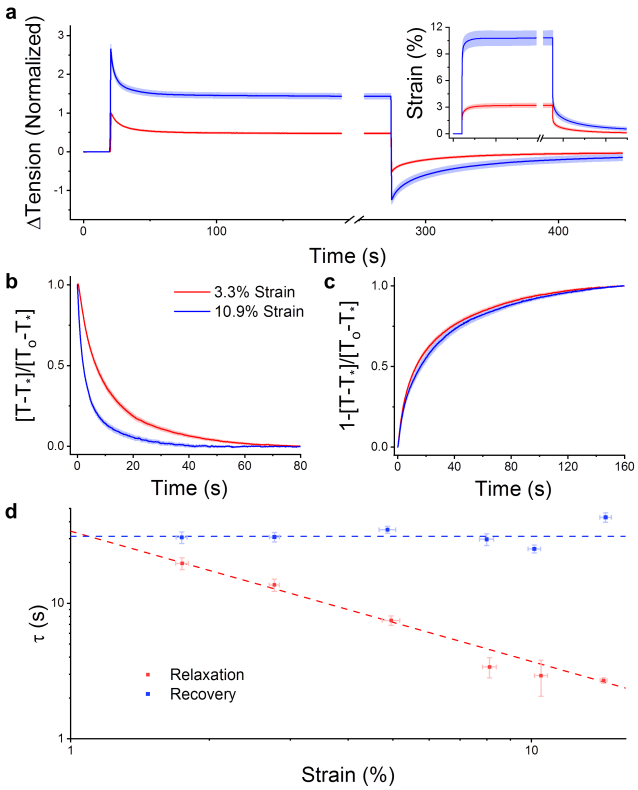

Fig. 3: The rate of stress relaxation was nonlinear while recovery was strain invariant. To assess viscoelastic non-linearity, the step size was varied (insert). Stress relaxations for a 3.3 and 10.9% step are shown in (a) (N=17). After normalizing for response amplitude, (b) shows that the rate of stress relaxation increased with strain. In fact, the time constant for stress relaxation appeared to follow an inverse power law with a near unity exponent (d). In contrast, the rate of recovery was invariant on the step size (c and d).

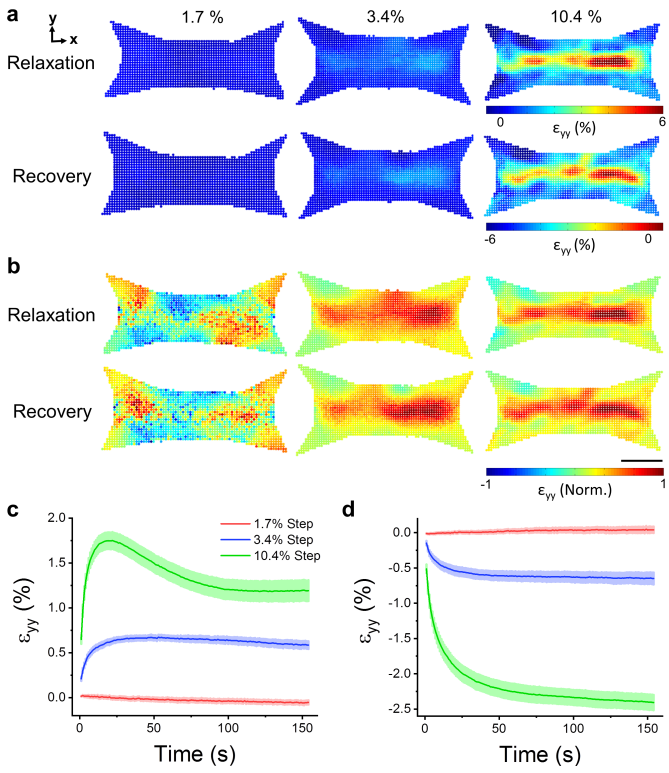

Fig. 4: The locations of remodeling following changes to microtissue length were strain-dependent. Spatial distributions of relaxation and recovery in the y-direction immediately after various step sizes are shown in (a). The distributions are normalized to three standard deviations outside of the absolute mean value in (b). The scale bar represents 100µm. The average (N=6) strain in the transverse direction that occurred during stress relaxation and recovery is plotted against elapsed time in (c) and (d), respectively.

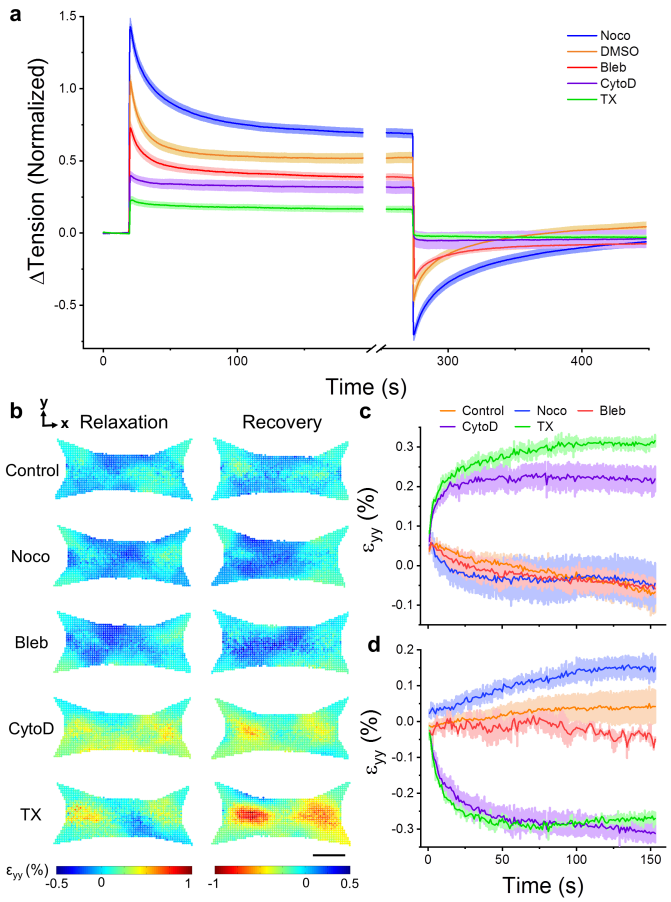

Fig. 5: Stress relaxation and recovery varied with pharmacological disruption of the cytoskeleton and myosin inhibition. Depolymerization of microtubules (Noco) increased stress relaxation and recovery responses, whereas myosin inhibition (Bleb), actin depolymerization (CytoD) and decellularization (TX) decreased relaxation and recovery (a). DMSO, a loading control, had no difference compared to no treatment. Microtissues only ever received a single treatment and each treatment was normalized to its pretreatment control. The spatial distributions of relaxation and recovery in the transverse direction following a small (1.7%) change in length are shown in (b). The scale bar represents 100μm. The average (N=3) strains in the transverse direction during stress relaxation and recovery are shown in (c) and (d), respectively.

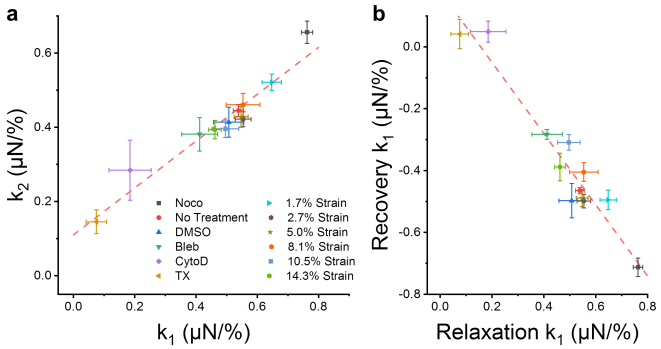

Fig. 6: The underlying relationships between microtissue dissipation and elasticity. The k_1 and k_2 stress relaxation spring constants were linearly coupled throughout an assortment of pharmacological treatments and step lengths (a) (linear regression; $P<0.001$ $R^2=0.94$). The amplitude of stress relaxation was also coupled to the amplitude of stress recovery (b) (linear regression; $P<0.001$ $R^2=0.92$).